RSC Advances

PAPER

View Article Online
View Journal | View Issue

Cite this: *RSC Adv.*, 2021, **11**, 18448

Synthesis of an urushiol derivative and its use for hydrolysis resistance in dentin adhesive

Ying Zhao,[a] Xi He,[a] Han Wang,[a] Jiufu Zhu,[b] Huimin Wang,[a] Yan Zheng,[b] Song Zhu*[a] and Zhanchen Cui *[b]

Hydrolysis resistance is essential to the durability of the dentin bonding interface. Urushiol is a natural monomer that has been used in different fields over thousands of years but has the disadvantage of a long drying time. In this study, we evaluated a novel photocurable derivative of urushiol as the main monomer for polymerization in dentin adhesive and its effect on hydrolysis resistance. The derivative was characterized by Fourier transform infrared spectroscopy and ^{1}H nuclear magnetic resonance spectroscopy. Compared with the Adper Single Bond 2, the experimentally synthesized adhesives had higher contact angles. In particular, the water sorption/solubility of the experimental samples were significantly lower than that of Adper Single Bond 2. The microtensile bond strengths of the test groups were higher than that of the control group, even after 5000 thermocycles. Cytotoxicity test results showed that adhesives based on the original derivative induced low toxicity to L929 cells. The results of this study may shift the focus of future research to natural monomers and even their derivatives which may perform well in dentistry.

Received 19th January 2021
Accepted 16th May 2021

DOI: 10.1039/d1ra00471a

rsc.li/rsc-advances

1. Introduction

Dental caries is a common disease in dentistry that is widely treated using an adhesive and composite resin.[1] Increasing the service life of restorative materials is becoming a major research focus. When the etch- and-rinse adhesive is used, after etching, the mechanical interlocking between the exposed network of collagen fibrils and the infiltrated monomers after polymerization form the 'hybrid layer', which contributes to the bond strength. But polymerization shrinkage of composite resin after curing leads to microleakage at the resin–dentin interface, creating a gap where saliva can enter and the bacteria in it can produce acid that activates MMPs and CTs.[2,3] These enzymes destroy collagens, triggering the degradation of the hybrid layer; consequently, this whole process of hydrolysis causes secondary caries, which is the major reason for the failure of composite restoration.[4] Because of the complex oral environment, which includes saliva and bacteria, hydrolysis resistance is important for these adhesives to be effective. To improve the durability of dentin adhesives, antibacterial ingredients, cysteine cathepsins and matrix metalloproteinase inhibitors, collagen cross-linkers and remineralization-promoting components are carried out extensive researches.[5–7] Bisphenol A-glycerolatedimethacrylate (Bis-GMA) as the main component is used in resin-based materials, but it is highly viscous because of the hydrogen bonding, a large quantity of hydrophilic monomers are required to dilute it, resulting in phase separation.[8,9] Bis-GMA is also more toxic than other monomers.[10] However, the ideal alternative monomer has not been explored to date.

Botanicals, which are antibacterial, antioxidant and anticancer with little drug resistance or side effects, are conventionally used as medicinal materials.[11–14] Lacquer sap is tapped from a common plant that mainly grows in Asia. The sap contains many different components, among which urushiol is the main compound.[15] Urushiol possesses hydrophobicity, flexibility and antibacterial activity as a coating material.[16,17] So it has been used for thousands of years in China to coat cultural relics and furniture, showing excellent aging resistance performance.[18] However, uses of urushiol are limited by the long time and very harsh conditions required for drying.[19] Therefore, modified derivatives with new chemical structures were synthesized to reduce the drying time.[20–23] Even though urushiol has antibacterial, anticancer, antioxidant and hydrophobic properties because of its catechol structure and alkyl chain, it is rarely used in dentistry.[16,24–26]

Urushiol nanofilm was used in dentistry to create a clear overlay on appliances that improved their durability by increasing the mechanical strength and intrinsic hydrophobicity while reducing the cytotoxicity for antimicrobial applications.[27] Moreover, 0.01% urushiol was reported to exhibit strong antibacterial capacity against *Streptococcus mutans* and had little effect on the shear bond strength of self-etch adhesives.[28] Likewise, urushiol exhibited as a cavity disinfectant and almost did not affect the adhesive microtensile bond strength in a class I cavity.[29] Thus far, urushiol

[a]*Department of Prosthetic Dentistry, School and Hospital of Stomatology, Jilin University, Changchun 130021, P. R. China. E-mail: zhusong1965@163.com*
[b]*State Key Lab of Supramolecular Structure and Materials, College of Chemistry, Jilin University, Changchun 130021, P. R. China*

has been mainly applied in dentistry for its antibacterial activity, with its other properties unexploited.

In this study, a original photocurable derivative of urushiol that had an immediate curing time was synthesized and applied to dentin adhesives with its hydrophobicity (Fig. 1). Different proportions of derivative were used to replace Bis-GMA when preparing total-etch adhesives. The hypothesis of this study was that the experimental adhesives would have higher hydrolysis resistance and persistent bond strengths than Bis-GMA containing adhesive.

2. Experimental

2.1 Materials

Urushiol was obtained from Wuhan National Lacquer Co., Ltd. (Wuhan, China). 2-Hydroxyethyl methacrylate (HEMA), camphorquinone (CQ), ethyl-4-dimethylaminobenzoate (4-EDMAB), triethyl amine and acryloyl chloride were purchased from Aladdin. The control, a commercial control adhesive, Adper Single Bond 2 (SB2), and a composite resin ESPE Filtek Z350 XT, were purchased from 3 M (St.Paul, MN, USA).

2.2 Synthesis of novel urushiol derivative

The structure of urushiol is shown in Fig. 2. Besides the basic structure, it consists of a side chain differing in the degree of unsaturation. The derivative was synthesized by an acyl chloride reaction, with ethyl acetate as a solvent and triethylamine as an acid-absorbing agent, as shown in Fig. 3. First, 12.92 ml acryloyl chloride was diluted with 20 ml ethyl acetate in a constant pressure funnel and was added dropwise to the reaction mixture of 17.89 ml urushiol, 150 ml ethyl acetate and 29.47 ml triethylamine at-10 °C, where a thermometer was used to monitor the temperature in real time. Acryloyl chloride was

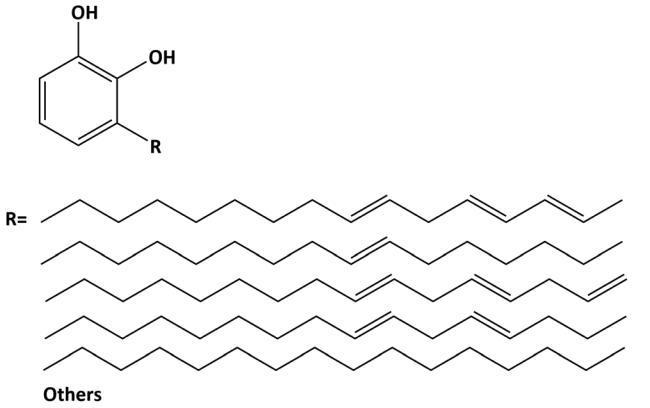

Fig. 2 General structure of urushiol; R represents a long unsaturated or saturated alkyl chain.

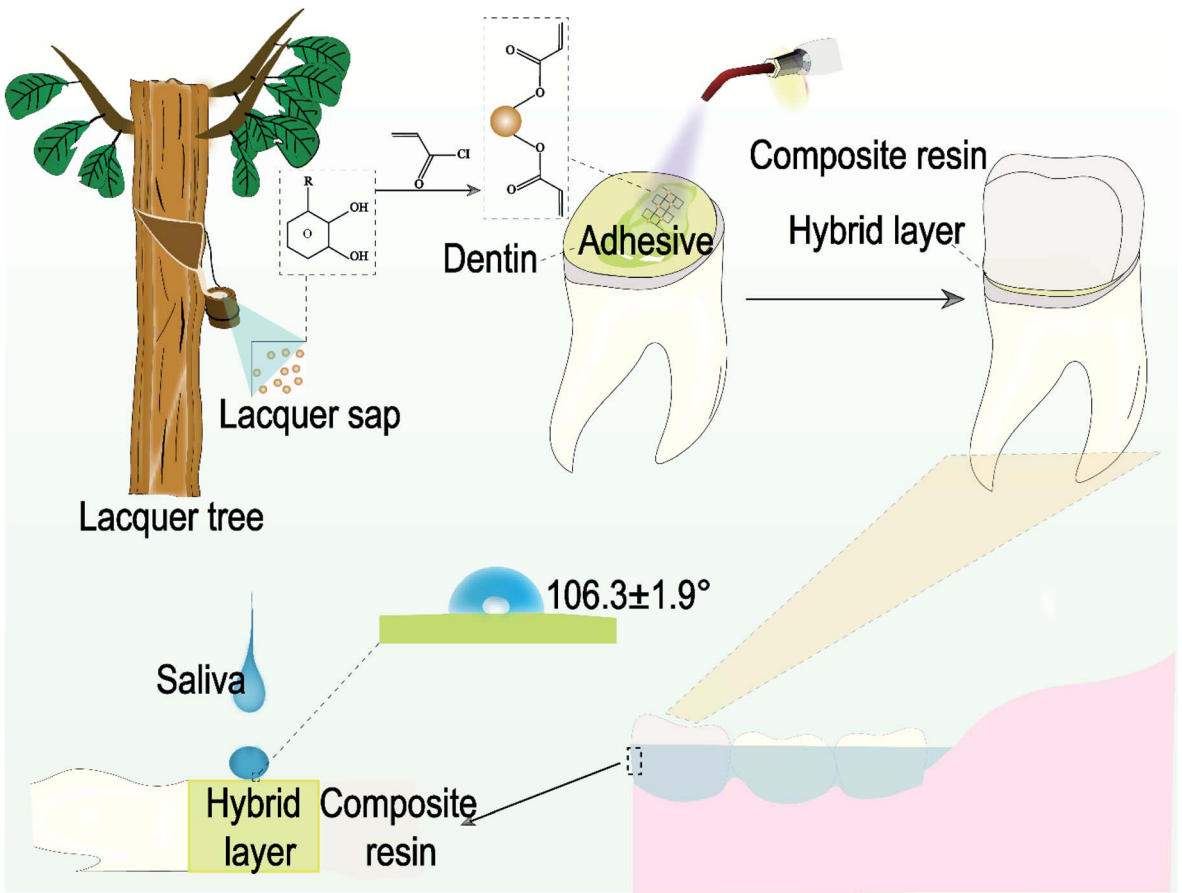

Fig. 1 Schematic diagram of experiment process and the advantage of the derivative.

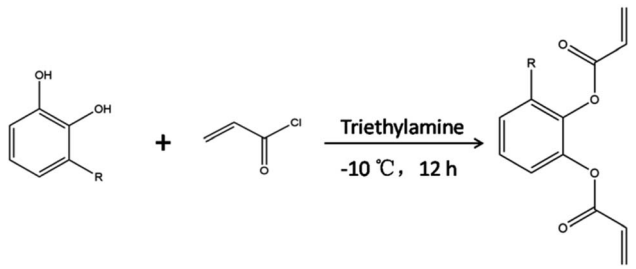

Fig. 3 Synthetic route of the urushiol derivative.

added in excess and the reaction was carried out under nitrogen for 12 h in a three-necked, round-bottomed flask equipped with a magnetic stirrer. Second, vacuum filtration, liquid separation, water removal and rotary evaporation were carried out on the product. Third, after simple separation and purification, the product was analyzed by thin layer chromatography. Finally, silica gel column chromatography was used to purify the product.

2.3 Characterization of the novel monomer

The optical properties of the purified derivative were characterized using Fourier transform infrared spectroscopy (FTIR) and ^{1}H nuclear magnetic resonance spectroscopy (NMR). The derivative was diluted with $CDCl_3$, and the monomer structure was characterized.

2.4 Evaluation of monomer thermal stability

The stability of the derivative after curing was tested by measuring the thermal transmission temperatures (T_g) with a differential scanning calorimeter (DSC TA Instruments DSC Q20). The temperature was increased from 40 to 200 °C at a rate of 10 °C min^{-1}.

2.5 Preparation of total-etch adhesives

Original photocurable total-etch adhesives were prepared by diluting the derivative with different quantities of HEMAs and mixing with photoinitiators (3% mass fraction, CQ and EDMAB) and ethanol (10% mass fraction). Four groups of adhesives containing different derivative contents are shown in Table 1.

2.6 Degree of conversion

The degrees of conversion (DCs) of four experimental adhesives and one commercial adhesive were determined by FTIR over a wavelength range of 500–4000 cm^{-1} at a resolution of 4 cm^{-1}, where 10 scans were performed with five samples of each group ($n = 5$). The adhesives were cured for 20 s, and FTIR scannings were performed before and after polymerization. An infrared absorption peak of the carbon–carbon double bonds at 1637 cm^{-1} (C=C) appeared, and the peak of the aromatic double bond at 1608 cm^{-1} was used as a reference. The DC was calculated using the following equation:

$$\mathrm{DC}\% = \left\{1 - \frac{(A_{1637}/A_{1608})\text{peak area after curing}}{(A_{1637}/A_{1608})\text{peak area before curing}}\right\} \times 100\%$$

Table 1 Formulation of the four types of experimental adhesives

	Monomers (wt%)		Other components (mol% of the monomeric phase)	
Groups	Urushiol derivative	HEMA	Photoinitiator	Ethanol
$U_{55\%}$	55	45	3	10
$U_{60\%}$	60	40	3	10
$U_{65\%}$	65	35	3	10
$U_{70\%}$	70	30	3	10

2.7 Contact angle measurement

Disc-shaped specimens (15 mm diameter and 1 mm thickness, $n = 5$) were fabricated for the five groups and tested. The contact angle was measured using a DataPhysics instrument (OCA-20, DataPhysics Co., Germany) and a 6 μl drop of deionized water, where both the left and right contact angles of the water drop were obtained.

2.8 Water sorption and solubility

ISO 4049:2009 was followed to determine the water sorption and solubility of the samples. Specimens were prepared as the same procedure used for the contact angle tests. Specimens were stored in a desiccator containing silica gel at 37 °C, and the silica gel was changed daily until the weights of specimens remained constant (M_1). The volume (V) of each specimen was calculated from electronic digital caliper measurements of the diameter and thickness. All specimens were immersed in distilled water at 37 °C for 7 d. The specimens were rinsed under running water, and filter paper was used to absorb water from the samples; the weight of sample was then determined (M_2). Finally, the specimens were redried in desiccators at 37 °C until weights of samples remained constant (M_3). W_{sp} and W_{sl} were calculated using the equations given below:

$$W_{sp} = \frac{M_2 - M_3}{V}$$

$$W_{sl} = \frac{M_1 - M_3}{V}$$

2.9 Microtensile bond strength (μTBS) and fracture mode

A total of 50 extracted caries-free human molars were stored in 0.5% chloramines-T at 4 °C within a month and prepared for a μTBS test. The protocol utilized in the present study [no. KT202003081] was reviewed and approved by the Ethics Committee for Human Studies of the School and Hospital of Stomatology, Jilin University, China. Teeth were cut from the coronal enamel using a low-speed saw under water for cooling to expose the occlusal dentin. The dentin was sanded under running water with 600-grit silicon carbide papers and teeth were randomly allocated into five groups (four groups of experimental adhesives and a Single Bond 2 group). After acid etching, specimens were rinsed with different adhesives and

cured for 20 s with an LED light. Two 2 mm thick layers of the commercial composite ESPE FiltekZ350 XT were built up on the dentinal surface. All specimens were soaked in distilled water at 37 °C for 24 h. Each tooth was cut perpendicularly to the bonded interface into sticks with a sectional area of approximately 1 mm^2 by a low-speed diamond saw (SYJ-150; Kejing Auto-Instrument, Shenyang, China). The μTBS was tested using a universal test machine (AG-X plus, Shimadzu Corporation, Japan) with a cross-head speed of 1 mm min^{-1}. The results were presented as the maximum load (N) divided by the interfacial area (mm^2).

The fracture mode was determined by observation with a stereomicroscope. Three sample types were observed. These types included interfacial adhesive failure, cohesive failure (including cohesive fracture of the dentin and the composite resin) and mixed fracture.

2.10 Morphology

The hybrid layer and resin tags were characterized using scanning electron microscopy (SEM; S4800, Hitachi Ltd, Tokyo, Japan). The samples were etched by a 37% phosphoric acid gel for 30 s and then immersed in a 5.25% sodium hypochlorite (NaClO) for 15 min. Finally, the samples were dehydrated with 50%, 70%, 90%, and 100% ethanol before dried in air. The specimens were sprayed with platinum and observed in the backscattered scanning detection mode at 5 kV.

2.11 Aging

One-half of the specimens used in the μTBS test ($n = 5$) were subjected to 5000 thermocycles (at 5 °C for 30 s and at 55 °C for 30 s) using a thermocycling instrument (PTC2c; Proto-tech, Portland, ME, USA).

2.11.1 μTBS test. The microtensile bond strengths of the specimens after thermocycling were determined following the procedure described above.

2.11.2 Nanoleakage. After thermocycling, the teeth were sectioned into slabs perpendicular to the bonding interface. Two slabs closest to the middle of teeth were selected and immersed in a 50 wt% ammoniated silver nitrate solution for 24 h. The slabs were rinsed and soaked in the photo development solution for 8 h under fluorescent light. All the specimens were polished with 1000-, 1200-, 1500-, 2000- and 2500- grit silicon carbide papers and ultrasonically cleaned with distilled water for 30 min. After natural air drying, the resin-dentin interface was observed under a SEM. The surfaces of specimens were characterized by energy dispersive X-ray spectroscopy (EDX).

2.12 Cytotoxicity test: cell counting Kit-8 and live/dead assay

The cured samples were placed in a 6-well plate and immersed into a culture medium with a superficial area of 6 cm^2 mL^{-1}. The extract was obtained from solution after 24 h and was diluted by 1000, 2000, and 4000 times.

L929 cells were used for the CCK-8 assay and incubated in 96-well culture plates at a density of 5000 cells per well using 100 μl of DMEM supplemented by 100 U mL^{-1} of penicillin, 100 μg mL^{-1} of streptomycin and 10% fetal bovine serum (FBS, Gibco, CA, USA) at 37 °C in 5% CO_2 for 24 h. After 24 h, the culture medium was replaced with 100 μl of the extract solution, which was prepared as described above. The cells were incubated for 1, 3 and 5 days. The CCK-8 assay was then carried out. The absorbance was evaluated at 450 nm with a microplate reader (Gene 5; BioTek Instruments, Winooski, VT, USA).

For the live/dead assay, L929 cells were seeded in 6-well culture plates at a density of 50 000 cells per well. After 24 h, the culture medium was replaced by diluted extract solution. The cells were stained using a Calcein-AM/PI double-stain kit (Beijing Solarbio Science Technology, Beijing, China) following the manufacturer's instructions. After staining, the live cells fluoresced green, and the dead cells fluoresced red. The cells were observed under a fluorescence microscope (Olympus IX71; Olympus) and the number of cells were measured using IMAGE J software (National Institutes of Health, Bethesda, Maryland, USA, http://imagej.nih.gov/ij/,1997e2014).

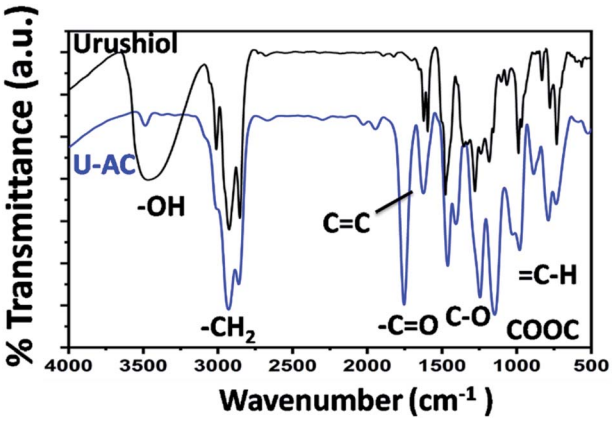

Fig. 4 FTIR spectra of the urushiol and the derivative. U-AC represents the FTIR spectra of the derivative.

2.13 Statistical analysis

The results were analyzed by ANOVA using SPSS software (version 19.0, SPSS Inc., Chicago, IL, USA). Test data with

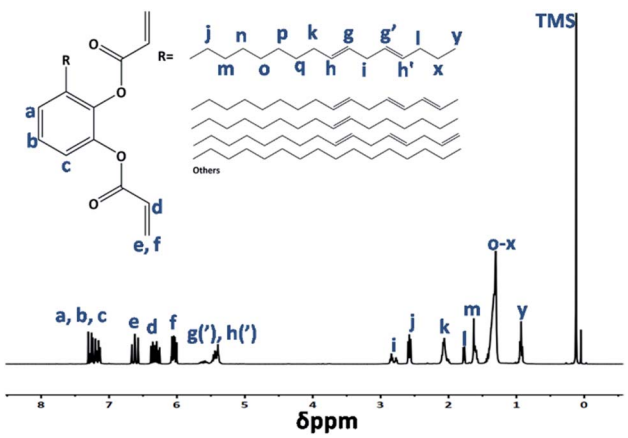

Fig. 5 ^{1}H NMR spectra of the derivative in $CDCl_3$.

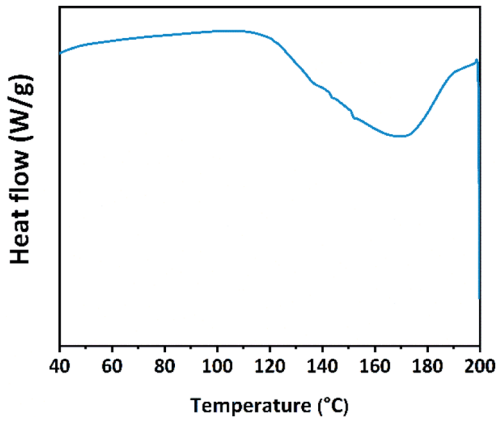

Fig. 6 DSC thermograms of polymerized derivative. Data were taken from the second heating cycle from 40 to 200 °C.

a normal distribution were analyzed using one-way ANOVA followed by Tukey's test and Dunnett's T3 test. The statistical significance level was set at 5% ($\alpha = 0.05$).

2.14 Ethics statement

The study was approved by the Ethics Committee of the School and Hospital of Stomatology at Jilin University. All the participating patients provided written informed consent.

3. Results and discussion

3.1 Characterization of urushiol derivative

Tests were performed to characterize the novel photocurable urushiol derivative for application in dentin adhesive. The chloride of the acryloyl chloride reacted with the hydroxyl group of urushiol producing the derivative containing two C=C bonds.

3.1.1 Fourier transform infrared spectroscopy. The FTIR spectra presented in Fig. 4 exhibited that the characteristic peak at 3400 cm^{-1} was corresponded to the –OH stretching vibration and peaks at 2930 cm^{-1} and 2855 cm^{-1} were corresponded to the –CH groups. After the reaction was carried out, the peak at 3400 cm^{-1} disappeared because –OH groups completely reacted with the acryloyl chloride. An absorption band appeared at approximately 1637 cm^{-1} corresponding to the C=C bond. The C–O stretching vibration appeared at approximately 1230 cm^{-1}. These bands indicated that the urushiol derivative was synthesized.

3.1.2 Nuclear magnetic resonance spectroscopy. The typical structure of the derivative was characterized by ^{1}H NMR spectra and is shown in Fig. 5. The signals in the range of 7.18–7.37 ppm corresponded to the hydrogens on benzene ring. The peak at 5.95–6.15 ppm and 6.55–6.75 ppm were attributed to the unsaturated hydrogens of carbon–carbon double bond at the end. Additionally, another unsaturated hydrogens of the bond appeared at 6.25–6.37 ppm. The peak at 5.35–5.5 ppm corresponded to the

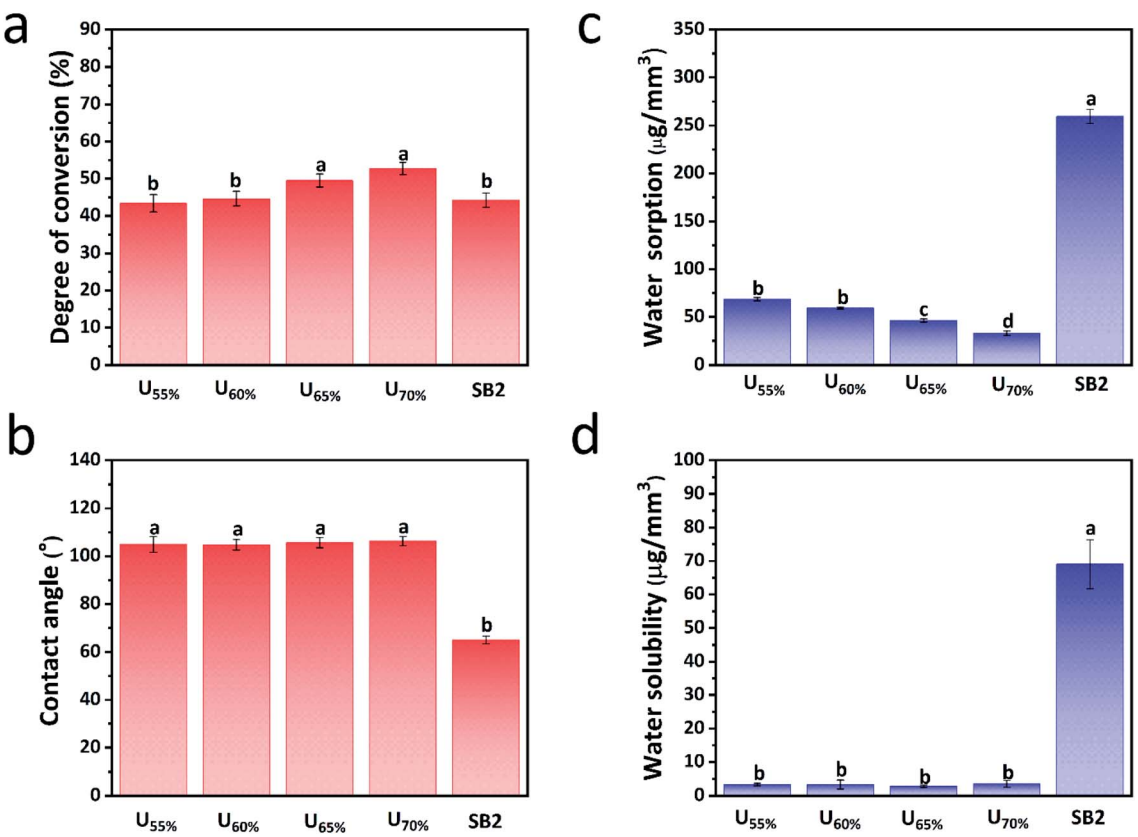

Fig. 7 Degree of conversion (a), contact angle (b), water sorption (c) and solubility (d) of the four experimental groups and control group. [a]Different lowercase letters represent statistically significant differences ($P < 0.05$).

unsaturated hydrogens of the side chain. Because R is a composition based on alkyl chain, other small distant peaks such as 0.85 ppm, 1.3 ppm, 1.6 ppm, 2.1 ppm, 2.6 ppm and 2.82 ppm were ascribed to the hydrogens of the side chain.

3.2 Thermal stability of the derivative

As shown in Fig. 6, inflexions corresponding to the glass transition temperature (T_g) of the polymerized derivative appeared in the temperature range from 40 to 200 °C. The benzene ring and the cross-linking of C=C bonds may lead to a high T_g. Many factors affect the thermal stabilities of polymers. High cross-linking may result in a high glass transition temperature.[30] Thermally stable restorative materials are required in a complex oral environment. The T_g of the polymerized derivative was 151.07 °C which is sufficient for oral use.

3.3 Degree of conversion

The degree of conversion is a measure of the degree of polymerization, which directly influences mechanical properties of materials.[31] A large quantity of monomers can drift away from an adhesive with a low DC leading to higher toxicity and even affecting gene expression.[32] As different monomers affect the DC, a new monomer should be tested before application.[33,34] The DC of Single Bond 2 was approximately 43%. Fig. 7a displays that experimental groups had higher degree of conversion than the commercial control, for which the results for group $U_{65\%}$ and $U_{70\%}$ were significantly different ($P < 0.05$) among the investigated groups. A higher content of C=C bonds may increase the DC.

3.4 Contact angle

As shown in Fig. 7b, the wettability of the adhesive interface after curing, which was measured by the static water. When the contact angle is higher than 90°, it manifests hydrophobicity of material after curing.

Single Bond 2 exhibited a contact angle of 65.06 ± 1.60°. The contact angles of experimental groups were all higher than 100°, indicating that experimental samples were hydrophobic after curing. The derivative consists of a benzene ring and a long alkyl chain, which are both hydrophobic groups. However, the C=C bonds in both the chain and the benzene ring of the derivative may lead to a higher degree of cross-linking than that in the commercial adhesive. The hydrophobic surface of the derivative prevents saliva water from easily infiltrating the adhesive interface.

3.5 Water sorption and solubility

The diluted monomer HEMA is the most frequently used type of monomer for adhesives, especially etch- and-rinse adhesives.[35] HEMA is hydrophilic and can absorb water.[36] Consequently degradations of the adhesive and collagen result from 'water tree'.[37] Mobile water in the 'water tree' causes unpolymerized monomers to drift away from the adhesive, and the resulting channels enable further degradation of the hybrid layer.[38] As the derivative is hydrophobic and has a low viscosity, the W_{sp} and W_{sl} of the experimental etch- and-rinse adhesives were significantly lower ($P < 0.05$) than those of the commercial adhesive (Fig. 7c and d).

Table 2 The microtensile bond strengths after 24 h and 6 m of the experimental groups and control group (MPa, $\bar{x} \pm s$, $n = 9$)[a]

Groups	24 h	6 m
$U_{55\%}$	28.56 ± 0.73^{Ac}	25.88 ± 2.94^{Bb}
$U_{60\%}$	$31.79 \pm 2.22^{Ab,c}$	$27.66 \pm 4.01^{Ba,b}$
$U_{65\%}$	39.00 ± 1.82^{Aa}	$28.51 \pm 4.11^{Ba,b}$
$U_{70\%}$	$35.80 \pm 1.21^{Aa,b}$	33.79 ± 2.31^{Aa}
SB2	26.53 ± 2.75^{Ad}	21.91 ± 2.92^{Bb}

[a] Different lowercase letters represent statistically significant differences within the same column ($P < 0.05$; vertical comparisons); different capital letters represent statistically significant differences within the same line ($P < 0.05$; horizontal comparisons).

The derivative content of the adhesive was increased from 55% to 70% in this study. The increasing content may be the reason that the W_{sp} of the experimental adhesives gradually and significantly decreased to a level lower than that of SB2 ($P < 0.05$). Fig. 7d displays that the W_{sl} of experimental groups are compliant with international standards. The degree of cross-linking in adhesives consisting of the derivative may be higher than that of the commercial control group, which may affect water dynamics.

3.6 Microtensile bond strength and failure mode

The microtensile bond strengths before and after aging are important indexes to assess the durability of adhesive materials.[39] In this study, 5000 thermocycles is considered to be equivalent to 6 months of service time. As shown in Table 2 the bond strengths after both 24 h and 6 m for experimental groups were higher than those of the commercial control group. After

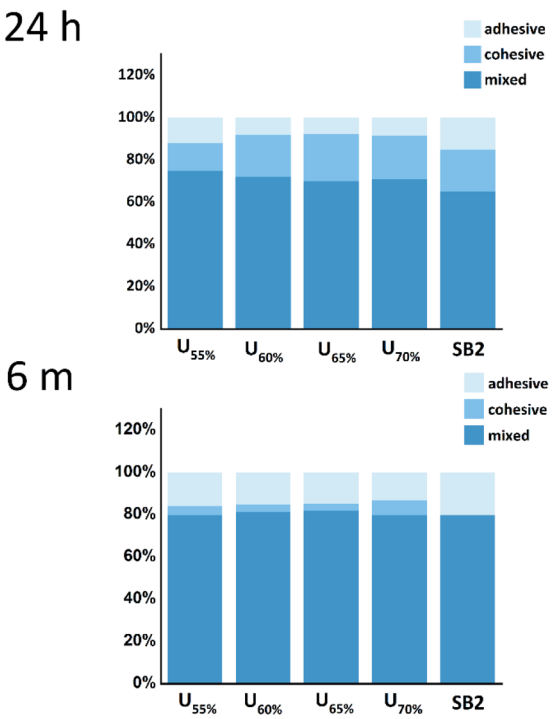

Fig. 8 Fracture mode of the samples in the μTBS tests after 24 h and 6 m.

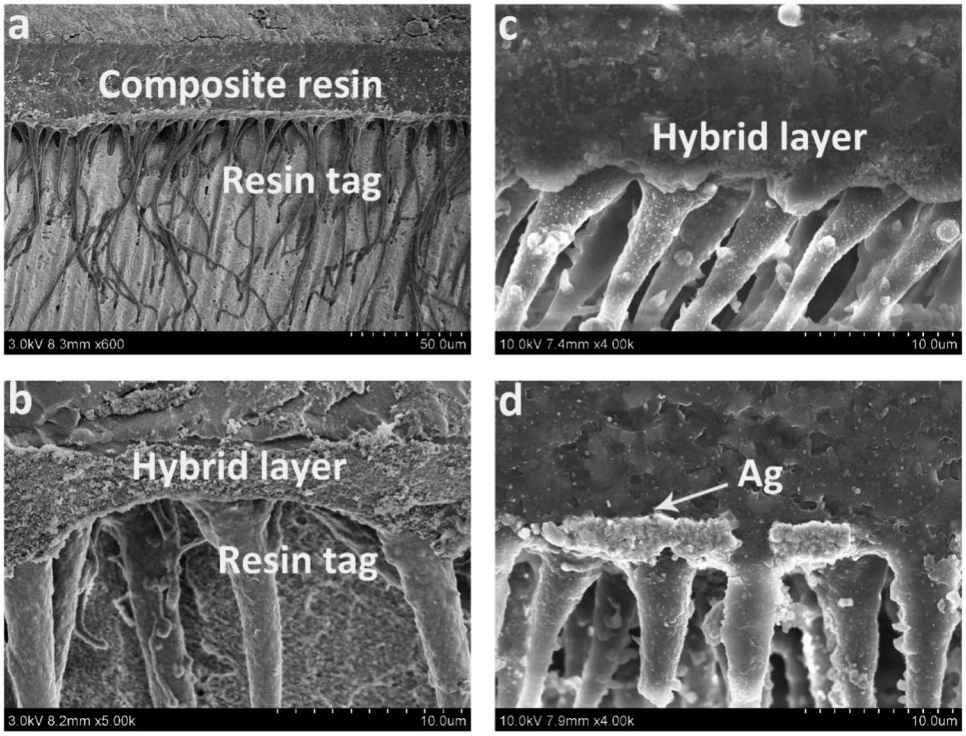

Fig. 9 SEM images of the resin tag (a) and hybrid layer (b) of the group $U_{70\%}$. Nanoleakage images of the group $U_{70\%}$ (c) and control group (d) by SEM.

immersed in water 24 h, microtensile bond strength of group $U_{65\%}$ was the highest. All the samples except these of group $U_{70\%}$ decreased significantly after aging process of 6 m ($P < 0.05$). So group $U_{70\%}$ was the most stable group displaying the highest performance during the aging. That might be caused by the little phase separation or not enough DC of the highly hydrophobic derivative in the μTBS test after 24 h. But because of the highest content of derivative, after 5000 thermocycles, group $U_{70\%}$ exhibited significantly higher performance than the other groups ($P < 0.05$). This result manifests that the hydrophobic derivative had better durability in a complex oral environment.

The uses of natural materials are becoming increasingly popular in medical fields. The natural monomer obtained from the lacquer sap is renewable and environmentally friendly. As dentin adhesives are photocurable or dual-curable, the ability to polymerize the derivative under blue light is critical. In this study, the original derivative was hydrophobic after polymerization, so the hydrolysis resistant property of the derivative is valuable for adhesive applications.

Mixed failure accounted for more than 70% of the total number of fractures in the five investigated groups before and after cycling as it showed in Fig. 8. This result shows that the novel derivative has better adhesion property. The number of interfacial fractures increased after cycling, and changes in the temperature and water content affected the hybrid layer.

3.7 Scanning electron microscopy

The resin tag also makes effects on the bond strength of the hybrid layer.[40] As shown in Fig. 9a and Fig. 9b, the hybrid layer was uniform and the resin tag was almost 100 μm long.

3.8 Nanoleakage

In 1995, Sano reported a pore with diameter less than 50 nm between the hybrid layer and dentin which was described as "nanoleakage".[41] The presence of water in the hybrid layer shows that external water can infiltrate the hybrid layer.[42] Nanoleakage occurs before microleakage and has more severe repercussions.[43] The silver nanoparticles in the control group appeared bright white in the SEM images.

As shown in Fig. 9c, the nanoleakage in group $U_{70\%}$ was less than that in the control group and that silver particles were found only in the hybrid layer. The energy dispersive X-ray spectroscopy results confirmed the presence of Ag on the surface of the control group (Fig. 10).

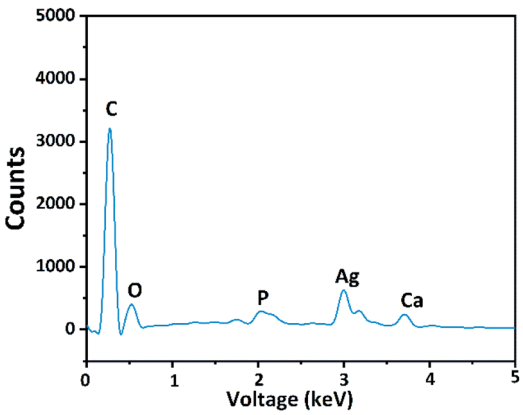

Fig. 10 Surface elemental analysis by energy dispersive X-ray spectroscopy (EDX).

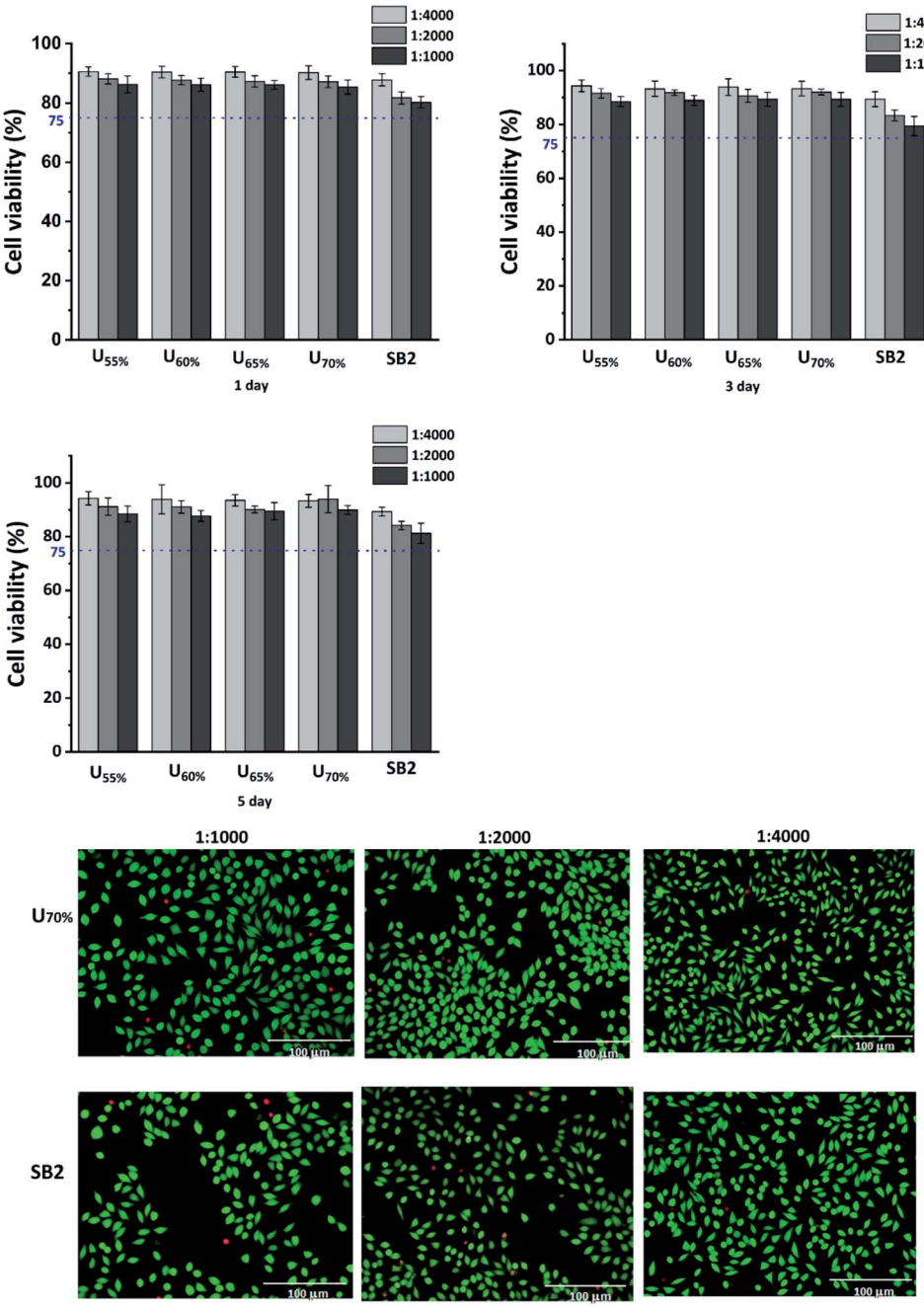

Fig. 11 Cytotoxicity of the experimental groups and control group in culture medium for 1, 3, 5 day were determined by CCK-8 assay; images of live/dead cell staining of L929 cells cultured for 24 h in culture medium (control) were compared with group $U_{70\%}$ at different dilutions (1 : 1000, 1 : 2000 and 1 : 4000 (v/v) dilutions); living cells were stained by calcium-AM (green), and dead cells were stained by PI (red); scale bar = 100 μm.

3.9 Cell cytotoxicity and morphology

L929 is an oral fibroblast and is the most common cell in the mouth. The components of dentin adhesives may be toxic to oral cells. The adhesive monomers may cause inflammatory responses in cells and even trigger apoptotic cell death.[44]

Fig. 11 displays that the proliferations of L929 cells in the experimental adhesives were not significantly higher than in SB2 after 24 h and were higher than 75%, indicating that the experimental adhesives induced less cytotoxicity than SB2 in oral cells. With the increasing culture time, the cytotoxicity of adhesives became a little lower. Cytotoxicity was evaluated by calculating the live cells and observing their adhesion. The live/dead assay results showed a lower cell density for the commercial group than that of experimental groups, which manifested the toxicities of the more unpolymerized monomers or solvents in SB2 with lower DC and higher W_{sl}. The results of ImageJ software in group $U_{70\%}$ and SB2 diluting 4000 times were 93.07 ± 4.65% and 84.53 ± 8.96%. The morphology of the live cells was uniform, and the cell adhesion of the commercial

group was worse than that of the experimental group too. The toxicities of SB2 components, such as Bis-GMA or HEMA have been proven.

4. Conclusions

In summary, the performance of the etch- and-rinse adhesive containing the urushiol derivative was evaluated for application in restorative materials. The results indicate that the original adhesive with derivative has suitable adhesion properties for application especially the group $U_{70\%}$. The derivative may increase the hydrolysis resistance and has acceptable biocompatibility. In future, the adhesive with 70% extent of the derivative will have a good performance in practical application. Furthermore, this study may broaden the horizon of application of natural monomers in dentistry.

Conflicts of interest

There are no conflicts to declare.

Acknowledgements

This study was supported by the Scientific and Technological Development Scheme of Ji Lin Province (Grant No. 20200201425JC). The authors would like to acknowledge all those who contributed to this study.

Notes and references

1 J. E. Frencken, P. Sharma, L. Stenhouse, D. Green, D. Laverty and T. Dietrich, *J. Clin. Periodontol.*, 2017, **44**(suppl 18), S94–S105.
2 C. T. W. Meereis, E. A. Münchow, W. L. de Oliveira da Rosa, A. F. da Silva and E. Piva, *J. Mech. Behav. Biomed. Mater.*, 2018, **82**, 268–281.
3 L. Tjaderhane, F. D. Nascimento, L. Breschi, A. Mazzoni, I. L. Tersariol, S. Geraldeli, A. Tezvergil-Mutluay, M. R. Carrilho, R. M. Carvalho, F. R. Tay and D. H. Pashley, *Dent. Mater. J.*, 2013, **29**, 116–135.
4 J. L. Ferracane, *Dent. Mater. J.*, 2013, **29**, 51–58.
5 A. Frassetto, L. Breschi, G. Turco, G. Marchesi, R. Di Lenarda, F. R. Tay, D. H. Pashley and M. Cadenaro, *Dent. Mater. J.*, 2016, **32**, e41–e53.
6 J. Cai, J. E. A. Palamara and M. F. Burrow, *Calcif. Tissue Int.*, 2017, **102**, 265–279.
7 J.-H. Jang, M. G. Lee, J. L. Ferracane, H. Davis, H. E. Bae, D. Choi and D.-S. Kim, *J. Dent.*, 2018, **75**, 58–64.
8 E. Asmussen and A. Peutzfeldt, *Dent. Mater. J.*, 1998, **14**, 51–56.
9 Y. Wang and P. Spencer, *J. Biomed. Mater. Res., Part A*, 2005, **75**, 580–587.
10 J. He and H. M. Kopperud, *Dent. Mater. J.*, 2018, **34**, 1003–1013.
11 X. Kuang, V. Chen and X. Xu, *BioMed Res. Int.*, 2018, **2018**, 6498932.
12 C. Zhong, N. R. Wall, Y. Zu and G. Sui, *Curr. Med. Chem.*, 2017, **24**, 3681–3697.
13 H. R. Preus, O. C. Koldsland, A. M. Aass, L. Sandvik and B. F. Hansen, *Acta Odontol. Scand.*, 2013, **71**, 1613–1619.
14 G. John, S. Nagarajan, P. K. Vemula, J. R. Silverman and C. K. S. Pillai, *Prog. Polym. Sci.*, 2019, **92**, 158–209.
15 R. Lu, M. Ono, S. Suzuki and T. Miyakoshi, *Mater. Chem. Phys.*, 2006, **100**, 158–161.
16 J. Lee, J.-M. Doh, H.-G. Hahn, K.-B. Lee and Y. Lee, *Surf. Interface Anal.*, 2017, **49**, 479–487.
17 N. Lone, I. W. Cheong, M. Cho, Y.-K. Hong, Y. S. Choi, S. Perumal, B.-T. Oh and J. Joo, *J. Coat. Technol. Res.*, 2017, **14**, 621–630.
18 P. J. Jin, Y. L. Hu and Z. B. Ke, *Microsc. Res. Tech.*, 2017, **80**, 1344–1350.
19 J. Xia, J. Lin, Y. Xu and Q. Chen, *ACS Appl. Mater. Interfaces*, 2010, **3**, 482–489.
20 C. Wang, Y. He, H. Zhou, R. Tao, H. Chen, J. Ye and Y. Zhang, *Int. J. Polym. Sci.*, 2015, **2015**, 1–6.
21 H. Watanabe, M. Takahashi, H. Kihara and M. Yoshida, *Langmuir*, 2019, **35**, 4534–4539.
22 X. Zheng, X. Xiong, J. Yang, D. Chen, R. Jian and L. Lin, *Chem. Eng. J.*, 2018, **333**, 153–161.
23 Y. Deng, W. Bai, X. Zhang, J. Chen, S. Wang, J. Lin and Y. Xu, *ACS Omega*, 2018, **3**, 4129–4140.
24 M. Wu, B. Zhang, L. Jiang, J. Wu and G. Sun, *J. Archaeol. Sci.*, 2018, **100**, 80–87.
25 H. S. Kim, J. H. Yeum, S. W. Choi, J. Y. Lee and I. W. Cheong, *Prog. Org. Coat.*, 2009, **65**, 341–347.
26 Z. Qi, C. Wang and J. Jiang, *Molecules*, 2018, **23**, 1074.
27 H. Jeong, Y.-A. Cho, Y. Cho, E. Kang, H.-w. Ahn and J. Hong, *ACS Biomater. Sci. Eng.*, 2016, **2**, 344–348.
28 H.-S. Cha and D.-H. Shin, *Dent. Mater. J.*, 2016, **35**, 147–152.
29 B.-R. Kim, M.-H. Oh and D.-H. Shin, *Dent. Mater. J.*, 2017, **36**, 368–373.
30 B. Yu, Y. Shi, B. Yuan, S. Qiu, W. Xing, W. Hu, L. Song, S. Lo and Y. Hu, *J. Mater. Chem. A*, 2015, **3**, 8034–8044.
31 K. Sato, K. Hosaka, M. Takahashi, M. Ikeda, F. Tian, W. Komada, M. Nakajima, R. Foxton, Y. Nishitani, D. H. Pashley and J. Tagami, *J. Adhes. Dent.*, 2017, **19**, 31–37.
32 M. Fujioka-Kobayashi, R. J. Miron, A. Lussi, R. Gruber, N. Ilie, R. B. Price and G. Schmalz, *Dent. Mater. J.*, 2019, **35**, 1173–1193.
33 M. Hanabusa, K. Yoshihara, Y. Yoshida, T. Okihara, T. Yamamoto, Y. Momoi and B. Van Meerbeek, *Eur. J. Oral Sci.*, 2016, **124**, 204–209.
34 A. S. Q. S. Fonseca, A. D. Labruna Moreira, P. P. A. C. de Albuquerque, L. R. de Menezes, C. S. Pfeifer and L. F. J. Schneider, *Dent. Mater. J.*, 2017, **33**, 394–401.
35 D. Dressano, M. V. Salvador, M. T. Oliveira, G. M. Marchi, B. M. Fronza, M. Hadis, W. M. Palin and A. F. Lima, *J. Mech. Behav. Biomed. Mater.*, 2020, **110**, 103875.
36 J. Perdigao, B. Van Meerbeek, M. M. Lopes and W. W. Ambrose, *Dent. Mater. J.*, 1999, **15**, 282–295.
37 R. M. Carvalho, J. S. Mendonca, S. L. Santiago, R. R. Silveira, F. C. Garcia, F. R. Tay and D. H. Pashley, *J. Dent. Res.*, 2003, **82**, 597–601.

38 M. C. Erhardt, M. Toledano, R. Osorio and L. A. Pimenta, *Dent. Mater. J.*, 2008, **24**, 786–798.
39 L. Breschi, A. Mazzoni, A. Ruggeri, M. Cadenaro, R. Di Lenarda and E. De Stefano Dorigo, *Dent. Mater. J.*, 2008, **24**, 90–101.
40 M. Yoshiyama, F. R. Tay, J. Doi, Y. Nishitani, T. Yamada, K. Itou, R. M. Carvalho, M. Nakajima and D. H. Pashley, *J. Dent. Res.*, 2002, **81**, 556–560.
41 H. Sano, T. Takatsu, B. Ciucchi, J. A. Horner, W. G. Matthews and D. H. Pashley, *Oper. Dent.*, 1995, **20**, 18–25.
42 M. Okuda, P. N. Pereira, M. Nakajima, J. Tagami and D. H. Pashley, *Oper. Dent.*, 2002, **27**, 289–296.
43 T. Pioch, H. J. Staehle, H. Duschner and F. Garcia-Godoy, *Am. J. Dent.*, 2001, **14**, 252–258.
44 K. L. Van Landuyt, T. Nawrot, B. Geebelen, J. De Munck, J. Snauwaert, K. Yoshihara, H. Scheers, L. Godderis, P. Hoet and B. Van Meerbeek, *Dent. Mater. J.*, 2011, **27**, 723–747.